Dynamic-force extraction for micro-propulsion testing: Theory and experimental validation

Chuansheng Wang, Changbin Guan, Xuhui Liu, Xudong Wang, Fei Li (iD), and Xilong Yu

View Online   **Export Citation**   **CrossMark**

ARTICLES YOU MAY BE INTERESTED IN

Drop hammer with high-speed thermal imaging
Review of Scientific Instruments **89**, 115104 (2018); https://doi.org/10.1063/1.5051357

A nozzle for high-density supersonic gas jets at elevated temperatures
Review of Scientific Instruments **89**, 113114 (2018); https://doi.org/10.1063/1.5051586

Interference sensor for ultra-precision measurement of laser beam angular deflection
Review of Scientific Instruments **89**, 115003 (2018); https://doi.org/10.1063/1.5042721

Dynamic-force extraction for micro-propulsion testing: Theory and experimental validation

Chuansheng Wang,[1,2] Changbin Guan,[3] Xuhui Liu,[3] Xudong Wang,[3] Fei Li,[1,a)] and Xilong Yu[1,2]

[1]*State Key Laboratory of High Temperature Gas Dynamics, Institute of Mechanics, CAS, Beijing 100190, China*
[2]*School of Engineering Science, University of Chinese Academy of Sciences, Beijing 100049, China*
[3]*Beijing Institute of Control Engineering, China Academy of Space Technology, Beijing 100190, China*

A dynamic-force extraction, based on the least-squares method, is proposed for micro-propulsion testing. Having modeled the displacement oscillation of a micro-newton torsional pendulum, the time evolution of the dynamic force may be calculated if the stand constants are well calibrated. According to the linear characteristic of the motion equation, a reconstruction of the dynamic thrust reduces to solving linear equations. The simulation analysis shows that the error is affected by the sensor noise and the low-pass filter as well as the sampling rate. Validation experiments were performed showing that this method reconstructs the dynamic force well up to 8 Hz with an error less than 15 μN. The noise-induced error moreover varies little with frequency. © *2018 Author(s). All article content, except where otherwise noted, is licensed under a Creative Commons Attribution (CC BY) license (http://creativecommons.org/licenses/by/4.0/).* https://doi.org/10.1063/1.5037365

I. INTRODUCTION

Accurately controlling satellites at highly precise attitudes and/or orbits is vital in space missions requiring gravitational-wave or gravity-field measurements. To satisfy these requirements, micro-newton thrusters, such as cold gas engines and electromagnetic thrusters, were studied. Directly measuring such small thrusts is nearly impossible because the thrust is so miniscule that the device is unable to response to the changes it causes. Different kinds of thrust stands have been developed to accurately measure their performance. These stands are based on the torsion balance,[1–4] vertical pendulum,[5] indirect counterbalanced pendulum,[6] double pendulum balance,[7] and even the magnetically levitated balance.[8] Thrust is deduced using balance displacement. The tools often employed for these measurements include laser interferometers,[9] fiber optic linear displacement system (LDS) sensors,[3] heterodyne interferometers,[7] capacitive sensors,[5] as well as linear variable differential transformer (LVDT) sensors,[1,2] all of which are susceptible to electromagnetic interference and radio frequency (RF) interactions when testing both laboratory DC and RF-powered plasma thrusters.[11]

Most of these balance displacement systems have great accuracy and resolution. For example, Jamison[1] measured thrusts as small as 86 nano-newtons and Soni[3] developed a stand with a resolution of 10 nN for steady force measurements. Jarrige[10] measured a cold gas thruster to a resolution of 20 nN and a measurement bandwidth (MBW) of 0.1 Hz. Increasing MBW decreases the resolution.

Nevertheless, the challenging performances demanded of high-precision thrusters are thrust level, accuracy, thrust noise, and dynamic response. For instance, micro-thrusters with a high-frequency bandwidth and low noise are essential for "drag-free" missions, such as LISA.[7–9,11,12] The required

thrust range is between 0 and 3 mN with a resolution below 0.1 and 1 μN and a noise level of 0.1–1 μN/Hz$^{1/2}$, in a frequency bandwidth range of 2–10 Hz.[12] To enlarge the MBW of the thrust stand, many researchers sought new methods to extract dynamic force. These methods may be divided into two categories: increasing eigenfrequency and dynamic modeling.

To increase the eigenfrequency of the stand, auxiliary equipment or a new design in controlling the stand system is required. Using two parallel metallic plates and a FP cavity, Canuto[12] developed a nano-balance with a 13.5-Hz resonance frequency and sub-micro-newton resolution. A large natural frequency made it suitable for dynamic measurements up to 2 Hz. Orieux[13] used a feedback control loop to increase the frequency of a pendulum balance up to 42 Hz despite its low sensitivity of 25 μN. This method is widely used for measuring thrust noise. Active control suppresses its resonance and reduces the noise by more than one order of magnitude,[7] which is significant for long-term stability. Hagiwara[14] developed a proportional–integral–derivative controller to suppress the displacement of the arm of the torsion balance during thrusts. Masuda[15] studied the sensitivity of the torsion pendulum. With strong magnetic damping, a feedback control system was used to achieve long torsional periods and high sensitivity for the balance at low frequency (e.g., 1 mHz).

The second category is dynamic modeling. By analyzing the equation of motion of the thrust stand, the time-dependent force can be calculated using mathematical methods and the displacement history of the balance. A typical method is based on derivation. During this process, the first differential (speed) and second differential (acceleration) of the displacement history, as well as the well-calibrated stand constants (e.g., inertia and spring coefficient) are used.[16,17] Displacement-sensor samples of high frequency and high resolution are required. Therefore, this method has an obvious drawback in that the derivative may incur large errors arising from coupled noise

---

a)Author to whom correspondence should be addressed: lifei@imech.ac.cn

89, 115110-1

in the displacement data. D'Souza[19] used wavelet and Fourier analyses to reduce noise and directly transformed the control differential equation into a difference equation. Once the displacement was measured, the corresponding force is obtained using this control equation.

In the current study, a method is proposed to reconstruct the dynamic force from the displacement data. It uses the property of superposition of the control equation solutions, a basic functional idea, and a least-squares (LS) method. Verification experiments were performed to study the applicability of this method as well as the relationship between error and noise.

II. MICRO-THRUSTER BALANCE SYSTEM

As in former studies,[1–4] the thrust stand used here is based on a torsion pendulum (Fig. 1). The measurement range of this stand is 1–3000 μN for steady-force measurements with an accuracy of ~1 μN under ambient noise.[18]

Its main components included a pendulum arm, calibration coil, damper, displacement sensor, and two flexural pivots (Riverhawk, 6004-600). Each pivot has a torsional spring rate of 1.92×10^{-4} Nm/deg. The displacement sensor is the most important component of this balance system. A capacitive sensor (Fogale, Mc900) having a range of 100 μm and an accuracy of 2 nm was used. This pendulum holds an axial load of up to 2 kg. The 50-cm length pendulum arm was used to balance gravity and converts the thrust into a displacement. Similar to reports in the literature,[20,21] the electromagnetic calibration technique was used here. A coil was fixed on the base plate opposite a magnet fixed to the arm. This coil is connected with a high-precision current source making a magnet–coil system supplying a known force from 2 to 10 000 μN. A damper, comprising a circular permanent magnet and a copper plate, operates based on Lenz's law but also acts as a counterweight.
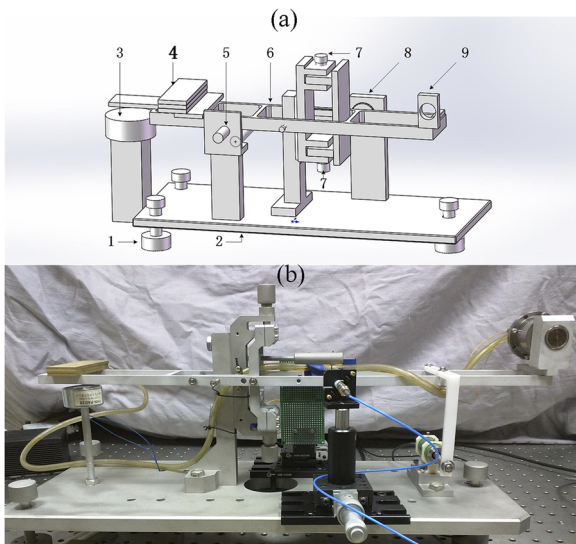

FIG. 1. (a) Schematic diagram of the balance: (1) leveling bolt, (2) base plate, (3) damping magnet, (4) counterweight and damping plate, (5) displacement sensor, (6) pendulum arm, (7) pivot axis (a couple), (8) calibration system, and (9) thruster mount and (b) photo of the balance.

Measurement and control systems and homemade software were developed to record and analyze the sensor signal, the on/off switching of the thruster, the change in distance between arm and sensor, and the magnet–coil gap. The gap ensures a reliable measurement of micro-thrusts in a vacuum chamber.

III. PRINCIPLE AND METHOD OF THE DYNAMIC-FORCE MEASUREMENT

A. Equation of motion of the pendulum

When the torsion pendulum undergoes small-angle swings, the motion of the pendulum arm follows the simple harmonic equation of forced vibration. The control equation is[22,23]

$$\mathrm{I}\frac{d\theta^2}{dt^2} + c\frac{d\theta}{dt} + k\theta = f(t)L, \qquad (1)$$

where θ represents the angular position relative to the initial position, L is the distance between pivot center and thrust action point, I (kg m^2) is the moment of inertia of the pendulum, c (N s m) is the damping constant, and k (N m/rad) is the spring constant. Setting

$$\zeta = \frac{c}{2}\sqrt{\frac{1}{Ik}}, \qquad (2)$$

$$\omega_n = \sqrt{\frac{k}{I}}, \qquad (3)$$

$$\omega_d = \omega_n\sqrt{1 - \zeta^2}, \qquad (4)$$

and substituting into Eq. (1) yields

$$\frac{d\theta^2}{dt^2} + 2\zeta\omega_n\frac{d\theta}{dt} + \omega_n{}^2\theta = f(t)\frac{L}{I}, \qquad (5)$$

where ζ is the coefficient of damping, ω_n is the natural frequency, and ω_d is the frequency of damped motion. For small deflections in our cases, the small-angle approximation may be used to deduce the angular deflection $\theta \approx x/L_s$, where x represents the displacement of the pendulum, and L_s represents the distance between the pivot center and the displacement sensor.

From theory, the amplitude of the pendulum obeys the amplitude-frequency function given by the magnification factor,[2,24]

$$\beta(s) = \frac{1}{\sqrt{(1 - s^2)^2 + (2\zeta s)^2}}, \qquad (6)$$

with relative frequency

$$s = \frac{\omega}{\omega_n}. \qquad (7)$$

Setting the coefficient of damping to 0.1, Fig. 2 plots the log-log relationship between the rate of amplitude amplification and relative frequency. In Ref. 25, Saulson found a frequency dependence to damping. Nevertheless, the coefficient of damping is treated as constant, independent of frequency as assumed in Refs. 16 and 19. For our situation, it is an appropriate assumption that is validated by experiments.

As can be seen, the amplitude ratio changes slightly at low frequencies and increases rapidly to a maximum value at the resonance frequency. At higher frequencies, the amplitude
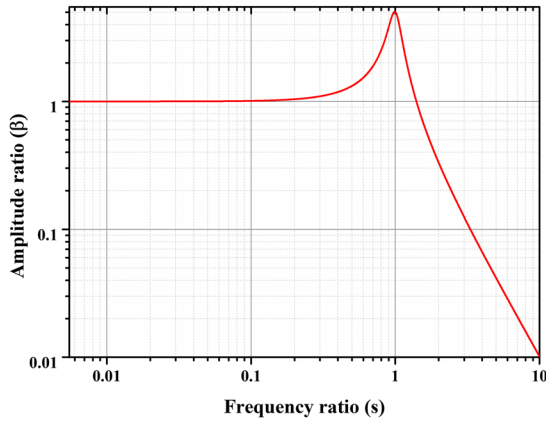
FIG. 2. Amplitude of the pendulum response versus relative frequency at $\zeta = 0.1$.

decreases rapidly; for example, it is 1% when the frequency is 10 times the natural frequency (Fig. 2).

B. Basic functional idea and the LS method

Based on the functional idea and the LS method, a new method for dynamic-thrust measurements is proposed. The unknown thrust can be reconstructed by solving Eq. (5). The basic functional idea used is to assume a force function expressed as $\{f_\tau\}$; here the curly braces signify a sequence of numbers with f_τ denoting any one of these numbers. That is,

f_τ defines the function that ensures Eq. (5) is expressible in theory and is here denoted by x_τ. The expression for x_τ contains f_τ, which means that x_τ is represented by f_τ. The theoretical solution of the displacement expressed by f_τ and the measured experimental values are used in the variance formula to find the function f_τ that makes the variance a minimum. That f_τ is the force that generates the displacement. Thus, this method seeks a functional solution for the force.

For a self-contained description of the method, the well-known LS method is described briefly here. The variance R of a function ϕ_j (e.g., the response of the balance to excitation), from the known data y_i (e.g., measured data of the displacement sensor), is defined as

$$R = \sum_{i=0}^{m} (\sum_{j=0}^{n} a_j \varphi_j(t_i - \tau_i) - y_i)^2, \tag{8}$$

where a_j are unknown coefficients (e.g., the dynamic force we want to measure), m represents the number of samples (e.g., number of displacement data), and n represents the number of a_j. Then seeking the extremum of the multivariate function, we have

$$\frac{\partial R}{\partial a_j} = \frac{\partial}{\partial a_j} (\sum_{i=0}^{m} (\sum_{j=0}^{n} a_j \varphi_j(t_i - \tau_i) - y_i)^2) = 0$$
$$j = 0, 1, 2 \ldots n \tag{9}$$

yielding

$$\begin{bmatrix} \sum_{i=1}^{m} \varphi(t_i - \tau_1)\varphi(t_i - \tau_1) & \cdots & \sum_{i=1}^{m} \varphi(t_i - \tau_n)\varphi(t_i - \tau_1) \\ \vdots & \ddots & \vdots \\ \sum_{i=1}^{m} \varphi(t_i - \tau_n)\varphi(t_i - \tau_1) & \cdots & \sum_{i=1}^{m} \varphi(t_i - \tau_n)\varphi(t_i - \tau_n) \end{bmatrix} \begin{bmatrix} a_1 \\ \vdots \\ a_j \\ \vdots \\ a_n \end{bmatrix} = \begin{bmatrix} \sum_{i=1}^{m} y_i\varphi(t_i - \tau_1) \\ \vdots \\ \sum_{i=1}^{m} y_i\varphi(t_i - \tau_n) \end{bmatrix}. \tag{10}$$

This set of linear equations for a_j is in a typical form to which the LS method applies. Measuring the dynamic force is achieved by adding the pendulum control equation, Eq. (5), and then applying the LS method, which is described next.

C. Dynamic-force extraction method

Figure 3 summarizes the basic process involved in reconstructing the dynamic force. Being a linear equation, Eq. (5) has the superposition property and has a theoretical solution for each special case. If the pendulum response $x(t)$ to the

FIG. 3. Steps in the extraction method. G.E governing equation, T.S theoretical solution, and L.E linear equations.

unit step input is known [Eq. (12)], it can be put into the LS method, Eq. (10), then used to replace the expression φ_j, and obtain Eq. (15) by linear rearrangement. By solving this linear system of equations, the dynamic force may be finally reconstructed.

In more detail, the method by which to extract the dynamic-force is based on discretization of the equations and the superposition of solutions of the governing equation. In Fig. 4, the continuous force can be assumed to be a sequence of superimposed forms of quasi-impulse actions $f(t) = \sum f_\tau \delta(t - \tau)$, where f_τ is the size of the impulse at $t = \tau$ and $\delta(t - \tau)$ is the unit impulse function.

Let the function $x(\tau)$ represent the theoretical solution at time τ, the time the impulse acts. An arbitrary displacement function takes the form
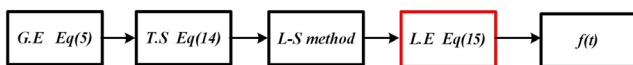
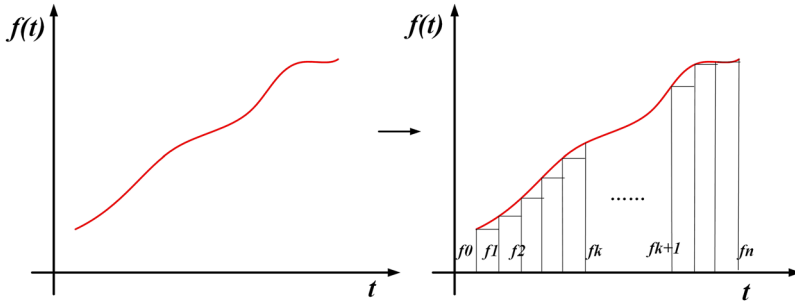$$x(t) = \sum x_\tau \delta(t - \tau). \tag{11}$$

FIG. 4. Sketch illustrating the discretization of a continuous function.

In practice, instead of the impulse function, a narrow rectangular impulse is used, having the benefit of overcoming interval limitations. In a damped balance system, the effect of the quasi-impulse is equivalent to a pair of time-inverted step functions. At time zero, the unit step function effect $x(t)$ is[24]

$$x(t) = \begin{cases} 0 & t \leq 0^-, \\ \dfrac{1}{\omega_n^2}\left[1 - e^{-\zeta\omega_n}(\cos(\omega_d t) + \dfrac{\zeta}{\sqrt{1-\zeta^2}}\sin(\omega_d t))\right] & t \geq 0^+, \end{cases} \tag{12}$$

where ζ, ω_n, and ω_d are the coefficient of damping, the natural frequency, and the frequency of damped vibration,

respectively. The quasi impulse becomes

$$\delta = x(t) - x(t - \tau). \tag{13}$$

Substituting Eq. (13) into Eq. (11) gives

$$x(t) = \sum_1^m f_\tau(x(t) - x(t - \tau)), \tag{14}$$

where $x(t)$ is the displacement, f_τ is the force at time τ, m is the number of points between the initial and final times. Substituting Eq. (14) into Eq. (10) gives

$$\begin{bmatrix} \sum\limits_{i=1}^m (x_1(t_i) - x_1(t_i - \tau))(x_1(t_i) - x_1(t_i - \tau)) & \cdots & \sum\limits_{i=1}^m (x_1(t_i) - x_1(t_i - \tau))(x_n(t_i) - x_n(t_i - \tau)) \\ \vdots & \ddots & \vdots \\ \sum\limits_{i=1}^m (x_n(t_i) - x_n(t_i - \tau))(x_1(t_i) - x_1(t_i - \tau)) & \cdots & \sum\limits_{i=1}^m (x_1(t_i) - x_1(t_i - \tau))(x_n(t_i) - x_n(t_i - \tau)) \end{bmatrix} \begin{bmatrix} f_1 \\ \vdots \\ f_j \\ \vdots \\ f_n \end{bmatrix} = \begin{bmatrix} \sum\limits_1^m (x_1(t_i) - x_1(t_i - \tau)) \\ \vdots \\ \sum\limits_1^m (x_n(t_i) - x_n(t_i - \tau)) \end{bmatrix}, \tag{15}$$

where x_i is the displacement function caused by the unit impulse at time t_i with τ its time of duration. Here f_i denotes the size of the impulse, i.e., the dynamic force; our target, which can be more positive or negative.

IV. EXPERIMENTAL

A. Experimental setup

To validate the dynamic-force extraction method, experiments were performed using the torsion balance (Fig. 1). During these experiments, the key issue is how to exert a known force on the balance for reference in comparison with the reconstructed forces. An electromagnetic calibration device [Fig. 5; labeled (8) in Fig. 1] was used to generate the external excitation. It has two components, a permanent magnet and a coil. The flat cylindrical magnet, made of rubidium nickel alloy, has a high magnetic energy density. Its superficial magnetic field intensity is about 4000 G. The circular hole in the core of the magnet makes it easier to fix on the side of

the pendulum arm. A special copper coil of radius 12.5 mm is placed facing parallel to the magnet (Fig. 5); its position and angle of pitch are precisely controlled using a 5-axis kinematic mount. Its center is coincident with the axis of symmetry of the magnet. A distance of 230 μm is maintained between magnet and coil.

With a resistance of about 0.6 Ω, this coil is connected in series with a 50-Ω resistance. A current-source-type signal generator is used to generate the different kinds of waveforms, corresponding to different dynamic forces. To avoid electric heating, the current is kept below 200 mA at an accuracy of better than 0.1 mA. After careful calibration, an oscilloscope is used to monitor the voltage/current of the coil for the known force.

The current-force coefficient can be measured using a high precision weighing balance. By placing the permanent magnet horizontally, the electromagnetic force between coil and permanent magnet can be measured by weighing the balance when the current changes. The rate of change between sensor output and force was deduced to be
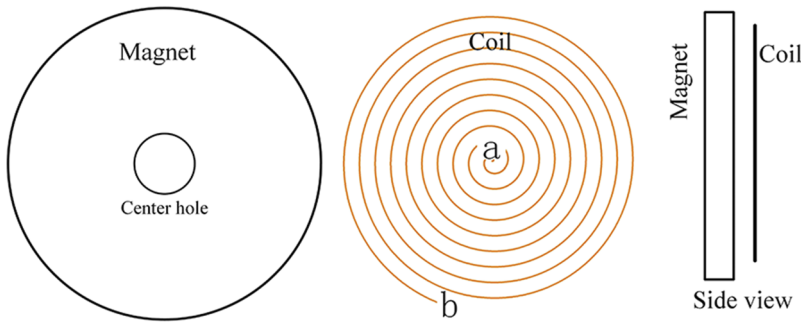
FIG. 5. Diagram of the electromagnetic calibration device.

202.15 μN/V in our experiments with an accuracy of about 1 μN.

Aided by this electromagnetic force generator, validation experiments were conducted with an arbitrary dynamic force. Three excitation waveforms were used to generate known dynamic forces, including square, sinusoidal, and sawtooth waveforms. The frequency range of these waveforms was from 0.05 to 10 Hz in intervals of 0.5 Hz and the amplitudes ranged from 120 to 300 μN. The sampling rate of the displacement sensor was set at 100 Hz.

B. Parameters calibration

One needs to know all the parameters including ζ, ω_d, and ω_n before Eq. (15) can be solved. To calibrate these parameters, modeling and measuring the vibration of the torsional pendulum is a feasible scheme. If $f(t) = 0$, Eq. (5) becomes a homogeneous differential equation. The measured displacement of the free vibration may be compared to its theoretical solution,

$$x = Ae^{-\zeta t} \cos(\omega_d t + \varphi), \tag{16}$$

where A and φ are determined by the initial conditions. The solution can be factored into an attenuation $x = e^{-\zeta t}$ and an oscillation $x = \cos(\omega_d t + \varphi)$. The frequency ω_d is obtained easily from the vibration period. The decay rate ζ can be deduced by taking the logarithm of the attenuation, $\ln(x) = -\zeta t$,

$$\zeta = \frac{1}{t_2 - t_1} \ln(\frac{x_1}{x_2}). \tag{17}$$

Hence, ζ is found using two or more points, with maximum displacements normally in different periods. In our experimental conditions, the values of these parameters were $\zeta = 0.69$, $\omega_n = 10.59$ rad/s, and $\omega_d = 7.66$ rad/s.

V. RESULTANT ANALYSIS

A. Typical reconstruction results

To verify the dynamic-force extraction method, three different waveforms for the coil current (corresponding to force) were applied to the torsional pendulum (Fig. 6). The initial phase of the input force is non-zero for better universality. The frequency of these input force waveforms was 0.1 Hz; the amplitude was 120 μN. The original displacement data and the reconstruction results (Fig. 7) show the responses of the damped pendulum to the various forces. In particular, in Fig. 7(b), damped oscillations had continued for more than 5 s. Hence, only the steady force lasting for about 10 s can be extracted using the conventional method. The time-dependence of the reconstructed force was found to coincide basically with the sawtooth input force [Fig. 7(c)], indicating that this method is feasible for dynamic-force extraction.

B. Influence of noise and sampling rate on dynamic-force measurements

1. System noise analysis

Apparently, noise in the displacement data has impacted on the reconstruction accuracy of the dynamic force. The inherent system noise, including balance and sensor, must be studied. A static experiment with no force loading was recorded for system-noise analysis. A fast Fourier transform (FFT) (Fig. 8) shows that the amplitude of noise varies with frequency. The downward sloping line is the linear fitting of the noise at low frequency (below 1 Hz) extrapolating the expected 1/f noise. At low frequency, the noise spectral density is mainly composed of signals from seismic motion.[16] At frequencies larger than the natural frequency (about 1.1 Hz), the noise is suppressed by the pendulum response (Fig. 2). In Fig. 8,
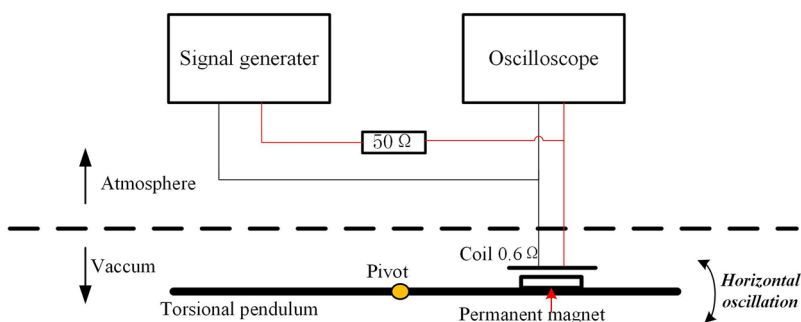

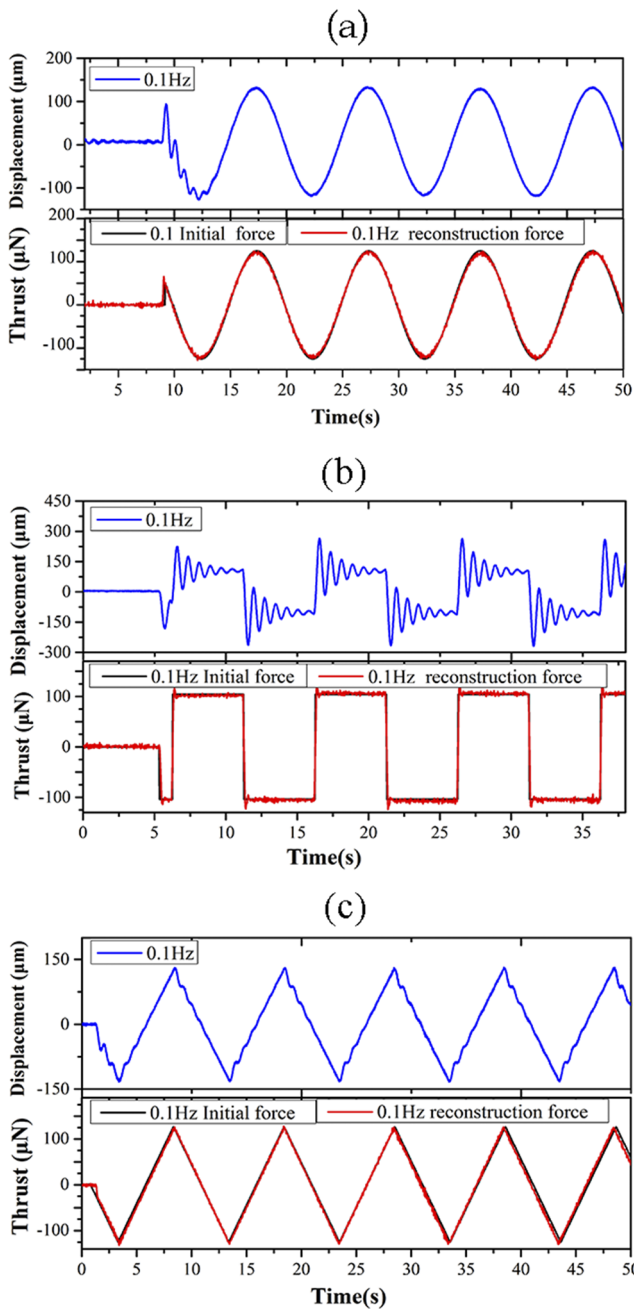FIG. 6. Diagram of the experimental setup.

(a)

(b)

(c)

FIG. 7. Displacement and reconstructed forces for the 0.1-Hz sinusoidal (a), square (b), and sawtooth (c) waveforms.

there is a clear peak around 10.5 Hz corresponding to the filter of the digital-to-analog converter for the displacement sensor.

2. Effect of noise and frequency

To study the effect of noise on the reconstructed force, a simulation analysis was performed in which noise was added to the theoretical displacement. The specific steps are as follows: First, a theoretical motion is simulated using Eq. (14) given the balance was excited by a sinusoidal force at a specific frequency. Then random white noise is added at the desired energy level to this theoretical motion and used as input data for the reconstruction program. Finally, the reconstructed force
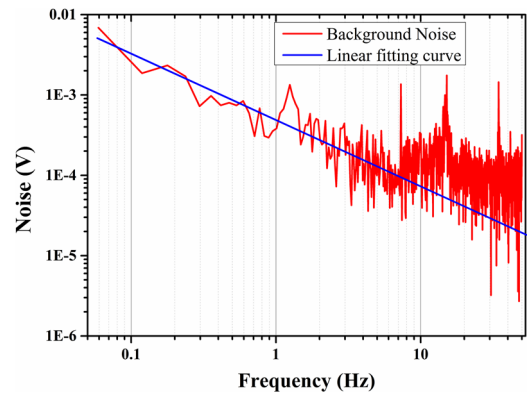

FIG. 8. FFT analysis of the system noise. Note that a low-pass filter ($f_c = 9.71$ Hz) was used in the reconstruction process to reduce the displacement noise at high frequencies. More details and analysis concerning the filter is given in the Appendix.

is compared with the initial sinusoidal force to analyze the accuracy.

A frequency range from 0.1 to 10 Hz for the sinusoidal driving force was used and the amplitude for the random noise was varied from 0 to 30 mV (0%–3%). Similar to the experimental data, artificial noisy data used to reconstruct dynamic force and measurement error may be calculated using the known sinusoidal forces. Figure 9 plots the relationship between reconstruct error (standard deviation) and noise level. The first feature to note is that error increases as noise levels rise for frequencies less than 8 Hz. At zero noise, the reconstructed force error is about 2 μN, whereas it is about 7.5 μN for 10 mV noise and 14.5 μN for 20 mV noise. The error deviation also increases as noise strengthens. It tends to zero in the absence of noise and less than 15 μN for a 20-mV noise level. The second feature of the error-noise relationship is that error increases notably when the frequency exceeds 8 Hz for all noise levels. This is caused by the low pass filter mentioned above. Here, the cutoff-frequency of the filter used is 9.71 Hz. It attenuates the input displacement signal with frequencies above 8 Hz (Fig. 12). Within the range of 8 Hz, the error remains nearly stable while the deviation in error increases slightly with frequency.
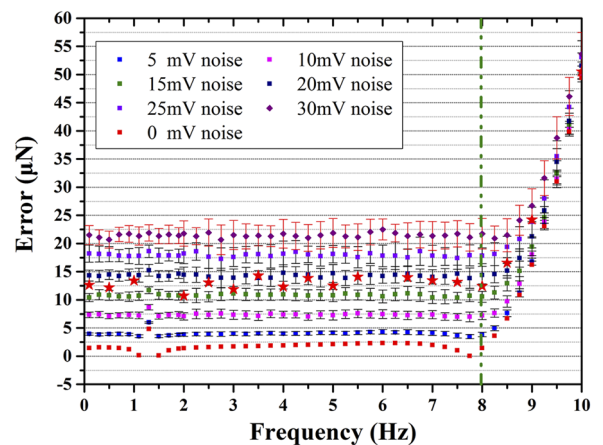

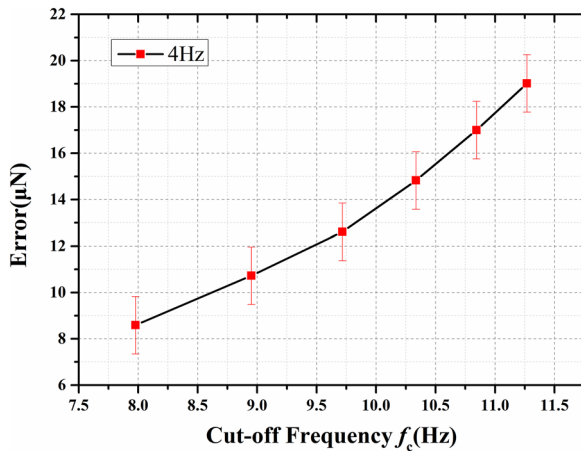FIG. 9. Reconstructed error versus frequency at different noise levels.

FIG. 10. Reconstructed error for different cut-off frequencies at fixed noise level of 17.5 mV.

The red stars in Fig. 9 mark the experimental results as for the results from the sinusoidal waveform [Fig. 7(a)]. Its trend with frequency coincides with the simulation results. For frequencies below 8 Hz, the error of the measured dynamic force is about 10–14 μN and insensitive to frequency.

3. Effect of cut-off frequency f_c

Figure 9 shows that for a given noise level, the extracted-force error almost remains constant from 0.1 to 8 Hz at fixed f_c of 9.71 Hz. For different f_c, this error changes. As shown in Fig. 10, for noise of 17.5-mV (approximate experimental noise), the force errors are about 8.5 μN and 19 μN for f_c of 8.0 and 11.2 Hz, respectively. The reconstructed force error increases rapidly as f_c increases.

4. Effect of sampling rate

The sampling rate of the displacement sensor may also influence the reconstruction accuracy. Subject to the same level of noise (10 mV, 1%), four sampling rates (100, 200, 500, and 1000 s^{-1}) were used in a simulation analysis to obtain the response (Fig. 11). The reconstruction results became better as the sampling rate increased. This is because at a high sampling rate, more displacement elements are used for the summation in Eq. (9), thereby reducing the equivalent noise. Nevertheless, the computation time of the reconstruction increased
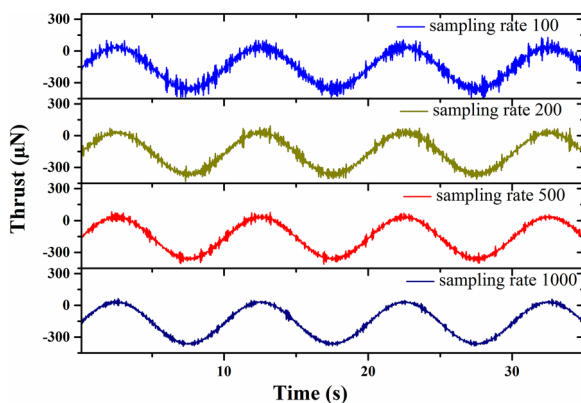

FIG. 11. Reconstruction result at different sampling rates.

significantly with the higher sampling rates. Therefore, it is best to reduce the sensor noise and choose an appropriate sampling rate.

VI. CONCLUSION

A mathematical method was proposed to extract the time-dependent force for micro-propulsion. A functional idea and LS method were used to reduce the measurements needed to solve the system of linear equations. Its main characteristic is that no auxiliary equipment is required. The MBW of the conventional torsion balance is improved significantly.

The dynamic-force extraction method and calibration of the stand parameters (i.e., ζ, ω_d, and ω_n) were studied. Validation experiments were performed using an electromagnetic device. The dynamic force was found to be well extracted from the oscillation of the balance with the reconstructed force coinciding with the known input force. Further simulation analysis shows that the reconstructed error increases as sensor noise or f_c increases. Moreover, the reconstruction results become better as sampling rates increase but at the expense of computation times. For the low-pass filter (f_c = 9.71 Hz) used, the MBW is up to 8 Hz and the error for the measured dynamic force is about 10–14 μN at a sampling rate of 100 Hz.

APPENDIX: THE IMPACT ANALYSIS OF THE FILTER PARAMETERS TO THE NOISE OF RECONSTRUCTION FORCE

A low-pass filter was used during reconstruction to reduce the displacement noise at high frequencies. A Butterworth-type filter was chosen because it has the smoothest passband attenuation. Five parameters were used in designing the filter, namely, passband frequency (PF), stopband frequency (SF), maximum attenuation of passband (MAP), minimum attenuation of the stopband (MAS), and frequency of sampling (FS). With the chosen parameter settings, the cut-off frequency (f_c) was estimated to have a 3-dB attenuation.

The amplitude-frequency function β (Fig. 2) determines the amplitude response of the pendulum under the dynamic force at different frequencies. The indication is that the displacement noise for different frequencies has different contributions to the error of the reconstructed dynamic force.

In analyzing the effect of the filter, a Fourier analysis of the displacement signal (with random white noise) provided the amplitude of the displacement noise at different frequencies. Divided by β, it represents a contribution to the error of the extracted force. From Fig. 12, a low-pass filter can remove the displacement noise of high frequencies and
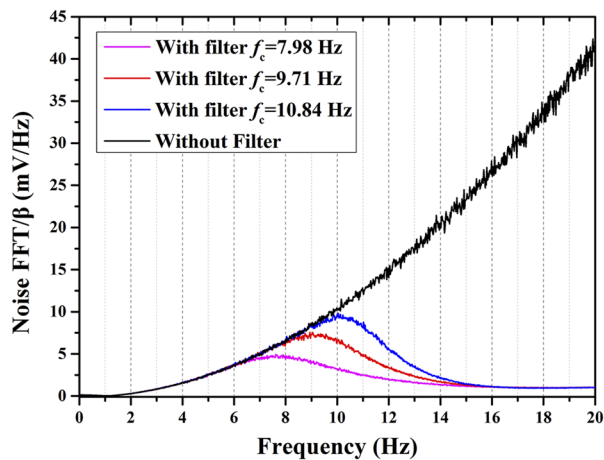
FIG. 12. Contribution of 17.5-mV white noise to the reconstructed force with/without filter.

decrease considerably the error of the reconstructed force. A lower f_c corresponds to a lower force error as also confirmed by Fig. 10. Nevertheless, a lower f_c loses dynamic information of the force. Therefore, f_c must be optimized to reach a compromise between dynamic-force accuracy and bandwidth. The filter parameter values chosen were PF = 40 rad, SF = 100 rad, MAP = 0.05 dB, MAS = 30 dB, and FS = 100 s^{-1} corresponding to f_c = 9.71 Hz. Hence, noise for frequencies above 8 Hz was removed (Fig. 12).

[1] A. J. Jamison and A. D. Ketsdever, "Gas dynamic calibration of a nano-Newton thrust stand," Rev. Sci. Instrum. **10**, 73 (2002).

[2] H. Koizumi, K. Komurasaki, and Y. Arakawa, "Development of thrust stand for low impulse measurement from micro-thrusters," Rev. Sci. Instrum. **75**, 3185 (2004).

[3] J. Soni and S. Roy, "Design and characterization of a nano-Newton resolution thrust stand," Rev. Sci. Instrum. **84**, 095103 (2013).

[4] M. Gamero-Castaño, "A torsional balance for the characterization of micro-Newton thrusters," Rev. Sci. Instrum. **74**, 4509 (2003).

[5] D. Packan, J. Bonnet, and S. Rocca, "Thrust measurements with the ONERA micronewton balance," in *International Electric Propulsion Conference* (University of Michigan, 2007), pp. 102–108.

[6] A. N. Grubisic and S. B. Gabriel, "Development of an indirect counterbalanced pendulum optical-lever thrust balance for micro to millinewton thrust measurement," Meas. Sci. Technol. **21**, 105101 (2010).

[7] F. G. Hey, A. Keller, U. Johann, C. Braxmaier, M. Tajmar, E. Fitzsimon, and D. Weise, "Development of a micro-thruster test facility which fulfils the LISA requirements," J. Phys. **610**, 012037 (2015).

[8] F. Mier-Hicks and P. C. Lozano, "Thrust measurements of ion electrospray thrusters using a cubesat compatible magnetically levitated thrust balance," in IEPC148, 2015.

[9] E. A. Cubbin, J. K. Ziemer, and E. Y. Choueiri, "Pulsed thrust measurements using laser interferometry," Rev. Sci. Instrum. **68**, 2339 (1997).

[10] J. Jarrige, P. Thobois, C. Blanchard *et al.*, "Thrust measurements of the Gaia mission flight-model cold gas thrusters," J. Propul. Power **30**(4), 934–943 (2014).

[11] S. J. Pottinger, D. Lamprou, A. K. Knoll, and V. J. Lappas, "Impact of plasma noise on a direct thrust measurement system," Rev. Sci. Instrum. **83**, 033504 (2012).

[12] E. Canuto and A. Rolino, "An automated interferometric balance for micro-thrust measurement," ISA Trans. **43**, 169–187 (2004).

[13] S. Orieux, C. Rossi, and D. Estéve, "Thrust stand for ground tests of solid propellant micro-thrusters," Rev. Sci. Instrum. **73**(7), 2694 (2002).

[14] K. Hagiwara, H. Yonamine, and H. Horisawa, "Control of thrust measurement system for CW laser thrusters," in The 32nd International Electric Propulsion Conference, Wiesbaden, Germany, September 11–15, 2011.

[15] M. Masuda, M. Sasaki, and A. Araya, "A torsion balance for probing a non-standard force in the sub-micrometre range," Classical Quantum Gravity **24**, 3965–3974 (2007).

[16] W. J. O'Neill, D. Lee, G. Anthony, and C. A. Alexeenko, "Dynamic modeling and experimental validation of thrust-stand for micro-propulsion Testing," AIAA Paper 2015-4186, 2015.

[17] L. Xu-hui, Y. Fei-hu, W. Yan-ming, J. Chen, X.-D. Wang, W. Mao, L. Fei, and Y. Xi-long, "Study of dynamic thrust measurement using torsional pendulum," J. Propul. Technol. **38**, 925–931 (2017).

[18] L. Fei, D. Guo, C. Wang, and X. Yu, "Micro-thrust measurements systems and their applications," in *LHD-CAS Summer Symposium* (Chinese Academy of Sciences, 2017), p. 147 (in Chinese).

[19] B. C. D'Souza and A. D. Ketsdever, "Investigation of time-dependent forces on a nano-Newton-second impulse balance," AIP Conf. Proc. **76**, 015105 (2005).

[20] H. Tang, C. Shi, X. Zhang, Z. Zhang, and J. Cheng, "Pulsed thrust measurements using electromagnetic calibration techniques"," Rev. Sci. Instrum. **82**, 035118 (2011).

[21] S. Rocca, C. Menon, and D. Nicolini, "FEEP micro-thrust balance characterization and testing," Meas. Sci. Technol. **17**, 711–718 (2006).

[22] J. E. Polk, P. Anthony, T. Haag, K. Scott, M. Walker, J. Blakely, and J. Ziemer, "Recommended practices in thrust measurements," in IEPC440, 2013.

[23] T. C. Lilly, A. P. Pancotti, A. D. Ketsdever, M. Young, and J. A. Duncan, "Development of a specific impulse balance for a pulsed capillary discharge," J. Propul. Power **25**(3), 823–826 (2013).

[24] J. Angeles, *Dynamic Response of Linear Mechanical Systems* (Springer Science Business Media LLC, 2011), p. 233.

[25] P. R. Saulson, *Fundamentals of Interferometric Gravitational Wave Detectors*, 2nd ed. (World Scientific, 2017).